Journal of Environmental Management xxx (2018) 1–12

Contents lists available at ScienceDirect

Journal of Environmental Management

journal homepage: www.elsevier.com/locate/jenvman

Research article

Photocatalytic activity of CuO/Cu(OH)$_2$ nanostructures in the degradation of Reactive Green 19A and textile effluent, phytotoxicity studies and their biogenic properties (antibacterial and anticancer)

Rijuta Ganesh Saratale [a], Gajanan S. Ghodake [b], Surendra K. Shinde [b], Si-Kyung Cho [b], Ganesh Dattatraya Saratale [c, *], Arivalagan Pugazhendhi [d], Ram Naresh Bharagava [e]

[a] Research Institute of Biotechnology and Medical Converged Science, Dongguk University-Seoul, Ilsandong-gu, Goyang-si, Gyeonggi-do, 10326, Republic of Korea
[b] Department of Biological and Environmental Science, Dongguk University, Ilsandong-gu, Goyang-si, Gyonggi-do, 10326, Republic of Korea
[c] Department of Food Science and Biotechnology, Dongguk University-Seoul, Ilsandong-gu, Goyang-si, Gyonggi-do, 10326, Republic of Korea
[d] Innovative Green Product Synthesis and Renewable Environment Development Research Group, Faculty of Environment and Labour Safety, Ton Duc Thang University, Ho Chi Minh City, Viet Nam
[e] Department of Environmental Microbiology, School for Environmental Sciences Babasaheb Bhimrao Ambedkar University, Vidya Vihar, 226 025, Uttar Pradesh, India

ARTICLE INFO

Article history:
Received 25 July 2017
Received in revised form
20 March 2018
Accepted 16 April 2018
Available online xxx

Keywords:
CuO/Cu(OH)$_2$ nanostructures
Photocatalytic degradation
Phytotoxicity studies
Tumor rat C6 cell line
TOC and COD
Antimicrobial activity
Textile effluent

ABSTRACT

In this study, CuO/Cu(OH)$_2$ (denoted as CuONs) nanostructures were synthesized relying to a cheap and rapid chemical co-precipitation method using copper sulfate and liquid ammonia as precursors. Results obtained from X-ray diffraction, and field emission scanning electron microscopy analysis revealed the crystalline nature of synthesized CuONs. Fourier transform infrared spectroscopy and energy dispersive spectroscopy studies showed interactions between copper and oxygen atoms. Synthesized CuONs showed the size in the range of 20–30 nm using high resolution transmission electron microscopy analysis. The photocatalytic degradation performance of Reactive Green 19A (RG19A) dye using CuONs was evaluated. The results showed that CuONs exhibited 98% degradation efficiency after 12 h and also complete mineralization in form of reducing chemical oxygen demand (COD) (84%) and total organic carbon (TOC) (80%). The nanocatalyst was recovered from the dye containing solution and its catalytic activity can be reused up to four times efficiently. CuONs was also able to decolorize actual textile effluent (80% in terms of the American Dye Manufacturers' Institute (ADMI) value) with significant reductions in COD (72%) and TOC (69%). Phytotoxicity studies revealed that the degradation products of RG19A and textile effluent were scarcely toxic in nature, thereby increasing the applicability of CuONs for the treatment of textile wastewater. Additionally, the CuONs showed a maximum antibacterial effect against human pathogens which also displayed synergistic antibacterial potential related to commercial antibiotics. Moreover, CuONs displayed strong antioxidant activity in terms of ABTS (2,2′-azino-bis(3-ethylbenzothiazoline-6-sulphonic acid) (IC_{50}: 51 μg/mL) and DPPH (1,1-diphenyl-2-picrylhydrazyl) (IC_{50}: 60 μg/mL) radical scavenging. The CuONs exhibited dose dependent response against tumor rat C6 cell line (IC_{50}: 60 μg/mL) and may serve as anticancer agents.

1. Introduction

Extensive research in the area of nanotechnology has grown to a higher extent attention and plays a ground-breaking role in modifying the molecular and atomic stages of materials. Materials reduced at nanometric scale display significantly different and exclusive characteristics and are extensively applied with variations in scientific fields (Saratale et al., 2017, 2018). Nanoscale metal oxide materials are considered as vital constituents in micro/nanoscale devices due to its certain specific size and size oriented physico-chemical characteristics. Cupric oxide (CuO) has become a widely accepted metal oxide because of a large surface area,

* Corresponding author.
E-mail address: gdsaratale@dongguk.edu (G.D. Saratale).

https://doi.org/10.1016/j.jenvman.2018.04.072
0301-4797/

remarkable magnetic and super-hydrophobic properties, being a *p*-type semiconductor having energy at slight band gap (1.2 eV), and also with superior catalytic activity and selectivity (Nezamzadeh-Ejhieh and Salimi, 2011; Filipič and Cvelbar, 2012). The copper oxide nanoparticles/nanostructures possess array of applications including its use in gas and bio-sensors, batteries, photodetectors, supercapacitors, solar cells, nanofluid, organic catalysis, super-hydrophobic surfaces, modification of electrode as non-enzymatic electrode, as well as for the elimination of organic contaminant (including dyes and heavy metals etc.) from waste water (Navaee and Salimi, 2017; Choi and Jang, 2010; Wang et al., 2011; Zhang et al., 2011; Amani-Beni and Nezamzadeh-Ejhieh, 2017; Maleki et al., 2015; Yavari et al., 2016). Furthermore, it has also shown excellent antimicrobial activity against various bacterial strains (Ren et al., 2009).

To increase the application of copper oxide nanostructures, their synthesis or preparation process should be simple, cost effective, scalable, and nontoxic in nature. There are many different approaches such as thermal oxidation, wet chemical methods, microwave irradiation, precipitation pyrolysis, sonochemical methods, thermal oxidation, and electrochemical methods were studied to synthesize different sizes and shapes of copper oxide nanostructures (CuONs) (Zhang et al., 2014; Phiwdang et al., 2013; Wongpisutpaisan et al., 2011). Different synthetic process such as hydrothermal and chemical precipitation are extensively used for the synthesis of CuONs. Precipitation methods are more advantageous due to less energy and temperature requirements, they are economically feasible low-cost, thus providing a good yield. These methods have been found to be effective to prepare CuONs for large scale production displaying property with controlled shape, configuration, and are being reproducible (Wang et al., 2011; Zhang et al., 2014; Phiwdang et al., 2013; Katwal et al., 2015; Nezamzadeh-Ejhieh and Zabihi-Mobarakeh, 2014).

In the current scenario, organic/synthetic dyes are widely applied in various industries such as textile dyeing, paper, pharmaceuticals, cosmetic ingredients, and in different sectors. It is reported that about 10,000 different textile dyes are regularly used in different industrial sectors (Saratale et al., 2011). It has been observed that about 280,000 tons which is about 15–50% of these dyes are expelled in form of industrial effluents worldwide every year. Among these dyes, azo dyes constitutes the largest class and constitutes about 70% of the total textile dyestuffs used (Sapkal et al., 2012; Buthiyappan et al., 2016). The release of textile and dye-house effluent causes abnormal coloration of the surface water, poor water quality, and eutrophication that directly affects the aquatic flora and fauna, thus poses a threat to environmental safety (Saratale et al., 2009; Bedekar et al., 2014). Photocatalytic degradation of these azo dyes involves cleavage of azo bond linkage that generates aromatic amines which are highly toxic, can be mutagenic and carcinogenic leads to have a great impact on human health (Salehi et al., 2016, 2017; Novotny et al., 2011). To treat dye wastewater, various common methods have been reported like: chlorination, coagulation, membrane separations, ozonation, electrochemical oxidation process, ion exchange, adsorption using activated carbon, and biological based methods (Houas et al., 2001; Sapkal et al., 2012; Saratale et al., 2011a, 2016).

Photocatalytic oxidation is an advanced oxidation process in which a photocatalyst is used to absorb light energy thereby completely mineralizing or neutralizing the organic contaminants. A number of metal oxides and metal ions were reported for the detoxification of various organic contaminants using photocatalytic processes (Houas et al., 2001; Kou et al., 2017; Akpan and Hameed, 2009; Derikvandi and Nezamzadeh-Ejhieh, 2017). This technique appears to be more effective for the treatment of this unsafe and toxic chemical compounds in wastes into nontoxic, safer degraded products under optimum environmental conditions (Mansouri et al., 2017; Gaya and Abdullah, 2008; Putri et al., 2016). In view of the advantages, we aimed to decolorize and degrade toxic, sulfonated azo dye RG19A and actual textile effluent using the synthesized CuONs. C.I. Reactive Green 19A is the most commonly used dye in different allied industries. To determine whether its degradation products could be less toxic in nature, we also checked the toxicity of its metabolites after photocatalytic degradation by CuONs. In the past two decades, a quick hastening in the ability to fight off against commercial antimicrobial agents have been observed, and so measurement of antibacterial activity of CuONs has become increasingly significant Rehana et al., 2017; Saratale et al., 2017, 2018. Moreover in view of their medicinal and technological uses, determination of antioxidant and anticancer activity of synthesized CuONS is required and which was addressed in this study.

The aim of this study is mainly focused on the preparation and characterization of synthesized CuONs. Besides, the photocatalytic degradation efficiency of CuONs for RG19A dye in aqueous solutions and actual textile effluent under UV light irradiation was investigated. Their mineralization was confirmed by chemical oxygen demand (COD) and total organic carbon (TOC) measurement, and the toxicity of the dye metabolites through degradation were evaluated by phytotoxicity studies. Additionally, to determine the potential antimicrobial applications of CuONs, we designed experiments to study their antibacterial effect against human pathogenic bacterial strains such as *Escherichia coli* and *Staphylococcus aureus*. In addition, the antioxidant potential and anticancer activity against tumor rat glial C6 cell lines of synthesized CuONs are also evaluated.

2. Materials and methods

2.1. Synthesis of copper nanostructures ($CuO/Cu(OH)_2$)

Copper sulfate pentahydrate ($CuSO_4 \cdot 5H_2O$) and liquid ammonia (NH_3) were used of analytical grade. Synthesis of CuONs nanostructures were performed using a co-precipitation method with a precursor such as copper sulfate and liquid ammonia. First, the precursor $CuSO_4$ was suspended in 100 mL of deionized water to form a 0.1 M concentration solution. Liquid ammonia solution was slowly dropped in a Teflon flask at 80 °C under vigorous stirring until the pH (pH 11) was achieved and then stirred for 2 h, which then turned to form a bluish black precipitate. The solution was further stirred continuously for a long period of time until the complete precipitation was achieved. The black precipitate obtained was centrifuged, washed thoroughly with number of times using distilled water followed by thrice with pure ethanol, and then dried at 80 °C for 16 h.

2.2. Characterization of synthesized CuONs

Structural measurements of the synthesized CuONs were carried out with an X-ray diffraction (Dmax III-A type, Rigaku Co., Japan) using Cu-Kα radiation (K = 1.54 A^o) and a scan range from 20° to 80° at 0.04° per min with a time constant of 2 s. The particle size was then calculated from X-ray diffraction (XRD) spectra using the Scherrer's equation. The size and morphology of the CuONs were examined by field emission scanning electron microscopy (FE-SEM) using a JEOL-64000 (Japan) connected to an attached energy-dispersive X-ray (EDX) spectroscope, and the phase identification of the sample was determined using XRD with Cu Kα incident radiation, a tube voltage of 40 kV, and a current of 30 mA. Fourier transform infrared (FTIR) spectra of CuONs recorded for the 4000–400 cm^{-1} range were made by the co-addition of 32 scans

Please cite this article in press as: Saratale, R.G., et al., Photocatalytic activity of $CuO/Cu(OH)_2$ nanostructures in the degradation of Reactive Green 19A and textile effluent, phytotoxicity studies and their biogenic properties (antibacterial and anticancer), Journal of Environmental Management (2018), https://doi.org/10.1016/j.jenvman.2018.04.072

with a resolution of 4 cm^{-1} using the instrument of PerkinElmer (Norwalk, CT, USA). The morphologies and size distribution of CuONs were determined by high-resolution transmission electron microscopy (HR-TEM) and along with this the patterns of selective area diffraction (SAED) were analyzed with Tecnai G2 20 S-TWIN (FEI Company, US) instrument. The average particle size of CuONs was measured from individual particles on the TEM images.

2.3. Photocatalytic degradation of dye RG19A by CuONs

To investigate the catalytic activity, 50 mL of dye RG19A aqueous solution (50 mg/L) was mixed and 200 mg/L of CuONs was added and sonicated for 10–15 min before dye addition to enhance the dispersion of the CuONs in the reaction mixture. The photocatalytic degradation of dye by CuONs was performed in a Vilber Lourmat Multilamp-photoreactor at room temperature at a UV-A wavelength at 365 nm having intensity 1000 μW/cm^2 at distance of 15 cm. The flask contain reaction mixture were put on the magnetic stirrer to get continuous stirring speed of 100 rpm. At specific time intervals, an aliquot (2 mL) of the reaction mixture was collected and centrifuged for the determination of absorbance with a UV–visible spectrophotometer (Optizen, Model 2120 UV plus) at a wavelength range of 300–800 nm. Initially, we checked the decolorization of RG19A performance using the synthesized CuONs.

Decolorization of RG19A using the synthesized CuONs was studied under various operational conditions: (*i*) UV irradiation without CuONs (photolysis), (*ii*) in the dark with CuONs (adsorption), and (*iii*) UV irradiation with CuONs (photocatalysis). Moreover, photocatalytic degradation efficiency of CuONs were analyzed to study the effect at different initial concentrations of RG19A (50–200 mg/L) while keeping a constant CuONs concentration (200 mg/L), and the decolorization effect of different concentrations of CuONs (100–500 mg/L) while keeping a constant RG19A concentration (100 mg/L). All the experiments of photocatalytic degradation studies were carried out in three sets.

The photodegradation of dye follows the pseudo first-order kinetics according to the Langmuir–Hinshelwood model, so the photodecolorization rate of each dye was studied by the following equation:

$$\ln C/C_0 = -kt$$

The rate constants (k) were calculated from the slopes of the straight-line segment of the plots of ln (C/C_0) versus t as a function of the used experimental parameters.

2.4. Reusability studies

To study the reusability of CuONs, after the complete degradation of RG19A under optimized conditions, the used particles were collected by centrifugation (6000 rpm for 15 min) from the reaction mixture. The separated CuONs were suspended in ethanol and acetone and were washed several times for use in the next cycle. The same procedure was repeated to 4 times. Experiments without CuONs (control) was also considered during the repeated batch studies for comparison under identical experimental procedures.

2.5. Photocatalytic degradation of actual textile effluent by CuONs

The actual textile effluent was passed through filter paper using Whatman no. 1 for separation of solid residues. Then the filtered effluent were taken in Erlenmeyer flasks (250 mL) and the flasks were autoclaved at 121 °C for 20 min to remove the microbial flora. The effluent was then diluted with a 1:1 proportion of sterile distilled water and used in the photocatalytic degradation by CuONs studies. A small amount of aliquots (about 2 ml) were collected at certain time intervals for analyzing color removal during photocatalysis. Similar conditions were applied for textile effluent without CuONs (control set) as mentioned above.

2.6. Phytotoxicity studies of RG19A, textile effluent, and their degraded products after photocatalytic treatment

The phytotoxicity of RG19A, actual textile effluent, and their degraded products after photocatalytic degradation was performed to study their toxic effects on common agricultural crops (*Sorghum vulgare* and *Phaseolus mungo*). RG19A, actual textile effluent, and their photocatalytically degraded products were extracted in ethyl acetate using solvent extraction method, evaporated and then dried. The dried degraded products were then suspended in distilled water so as to make a final concentration of 400 ppm. The phytotoxicity experiments were performed at room temperature (~28 °C). Ten seeds of *S. vulgare* and *P. mungo* plants were sown into a plastic sand pot and watered separately with 5 mL per day of RG19A (400 ppm), actual textile effluent (diluted 1:1), and at a similar concentration of metabolites of dye and actual textile effluent (400 ppm) which were acquired after photocatalytic degradation by CuONs. A control set using distilled water was also maintained and the seeds were watered with 5 mL every day. Phytotoxicity effect was determined by measuring the germination rate, plumule and radicles length of seedling growth of the plants after a week by using the method as reported in (Saratale et al., 2016).

2.7. Antibacterial activity of CuONs

In this study the antibacterial efficacy of synthesized CuONs was tested against *Staphylococcus aureus* and *Escherichia coli* as different human pathogenic bacteria using a disc diffusion assay using the procedure reported earlier (Saratale et al., 2017). In brief synthesized CuONs sample was loaded at a concentration of 50 μg CuONs/disc onto a sterile Whatman No. 1 paper discs (5 mm diameter). Following this, under sterile conditions, the discs were air-dried and finally retained on Luria–Bertani agar plates already loaded with microbial cultures using cotton swab and incubated overnight at 37 °C in bacteriological incubator. In addition to this, the synergistic antibacterial performance of synthesized CuONs was compared with commercial standard antibiotics: amoxicillin, oxytetracycline, and vancomycin (the standard antibiotic discs were obtained from Liofilchem, Italy) against *S. aureus*, and *E. coli.* The zone of inhibition (diameter in mm) were calculated surrounding the paper discs.

2.8. Antioxidant potential of CuONs

The free radical scavenging activity of the CuONs was determined with DPPH (2,2-diphenylamine-1-picryl hydrazyl) and ABTS salt (2,2′-azino-bis(3-ethylbenzothiazoline-6-sulphonic acid) as a free radical as per the reported method in our previous studies (Saratale et al., 2017). The assay containing the reaction mixture of DPPH solution (about 2 mL) and CuONs (0.2 mL) at different concentrations was vortexed and further incubated in dark at room temperature for 30 min in order to allow DPPH radical scavenging to take place. Then by keeping the catechol as a standard solution, the absorbance for the above reaction mixture was determined at 517 nm. For ABTS assay, ABTS salt (2,2′-azino-bis(3-ethylbenzothiazoline-6-sulphonic acid, (7.0 μM) and potassium persulfate (2.45 μM) were mixed together to form $ABTS^+$ by placing the solution in the dark for 16 h at 25 °C. The resulted solution of

Please cite this article in press as: Saratale, R.G., et al., Photocatalytic activity of CuO/$Cu(OH)_2$ nanostructures in the degradation of Reactive Green 19A and textile effluent, phytotoxicity studies and their biogenic properties (antibacterial and anticancer), Journal of Environmental Management (2018), https://doi.org/10.1016/j.jenvman.2018.04.072

$ABTS^+$ was diluted with ethanol (80%, v/v) to attain the absorbance 0.70 at 734 nm by a spectrophotometer (Moldovan et al., 2016). Solution was then diluted with various concentrations of CuONs (each 0.2 mL) and mixed with $ABTS^+$ solution (2 mL) then further immediately vortexed for 10 s and again after 6 min. Later, by taking ascorbic acid as a standard the absorbance was recorded spectrophotometrically at 734 nm. Each assay always contained a control set (without CuONs) throughout the experiment. All assays were carried out in three sets. The results in form of IC_{50} values (effective concentration that display 50% inhibition) were shown. The percentages of the DPPH and $ABTS^+$ scavenging radicals by the CuONs were determined using the method as reported earlier (Saratale et al., 2017).

2.9. Anticancer activity of CuONs against rat glial tumor C6 cell

The anticancer effect of CuONS were analyzed by treating with rat glial tumor C6 cell purchased from American Type Culture collection (ATCC). The anticancer activity of the CuONs was determined in C6 cell lines. The cell viability assay was carried out following the standard procedure of MTT assay which is described recently (Saratale et al., 2018). During this assay positive control of Doxorubocin (DOX) was added at concentration of 25 μg/mL. The percentage of cell viability was calculated which determines the anticancer potential of CuONs. In this study for each concentration three replicates were used.

2.10. Analytical studies

For MTT assay the cell viability readings were read by multi-well plate reader at 595 nm (Biotek, Epoch microplate spectrophotometer, Winooski, USA). Photocatalytic degradation of RG19A was quantitatively analyzed using a UV–visible spectrophotometer (Hitachi U-2800). To determine the degree of mineralization of RG19A before and after photocatalytic degradation using CuONs the reduction in total organic carbon (TOC) and chemical oxygen demand (COD) was determined (APHA, 1998). Under similar conditions with the test, a control using distilled water was used throughout the experiment and the complete procedure for TOC and COD is mentioned in our earlier study (Saratale et al., 2009). Similar procedures were employed for the textile effluent studies. For the dye wastewater study, the true color level independent of hue was measured using the American Dye Manufacturers' Institute (ADMI 3WL) tristimulus filter method (Saratale et al., 2011a). The ADMI removal ratio (%) of textile effluent before and after photocatalytic treatment is calculated as follows:

$$\text{ADMI removal ratio } (\%) = \frac{\text{Initial ADMI}_{(0\ \text{h})} - \text{Observed ADMI}_{\text{t}}}{\text{Initial ADMI}_{(0\ \text{h})}} \times 100\%,$$

where $ADMI_{(0\,h)}$ and $ADMI_{(t)}$ are the initial ADMI value (at 0 h) and the ADMI value after a particular reaction time (t), respectively.

2.11. Statistical analysis

All biological data were analyzed by one-way analysis of variance (ANOVA) followed by Tukey's HSD test. A threshold of $P = 0.05$ was considered significant to assess differences among means.

3. Results and discussion

In the present work, we proposed a chemical co-precipitation synthesis of CuONs using copper sulfate and liquid ammonia as precursors. The resulting CuONs were characterized using various analytical techniques (XRD, FTIR, FE-SEM, EDX spectroscopy, and HR-TEM) for the determination of size, shape and surface morphologies of the synthesized CuONs.

3.1. Characterization of synthesized CuONs

Fig. 1a shows X-ray diffraction (XRD) patterns of CuONs synthesized via the proposed chemical co-precipitation method; the all plot of the prepared material shows a mixed monoclinic phase of $CuO/Cu(OH)_2$ materials. The detected diffraction peaks of the monoclinic phase of $CuO/Cu(OH)_2$ materials were found at different diffraction angles: 22.74°, 28.04°, 32.20°, 33.42°, 35.50°, 39.12°, and 53.34° corresponding to the lattice planes (021), (112), (110), (002), (002-111), (111-200), and (150,132) of the monoclinic CuONs phase (JCPDS card No. 80-1917), respectively (Nezamzadeh-Ejhieh and Hushmandrad, 2010). The perfect peak intensities identified clearly matched the mixed crystalline structure of $CuO/Cu(OH)_2$, and no additional phase was observed. The intensity of plane (002-111) was found to be the largest of all the other peaks observed in the diffraction pattern of synthesized CuONs.

The crystallite size is calculated using the well-known Scherrer formula given below:

$$D = \frac{0.9\lambda}{\beta \cos\theta}, \quad (1)$$

where D is the crystallite size, λ is wavelength of Cu-K_α radiation, β is the full width at half maximum, and θ is the Bragg angle. The

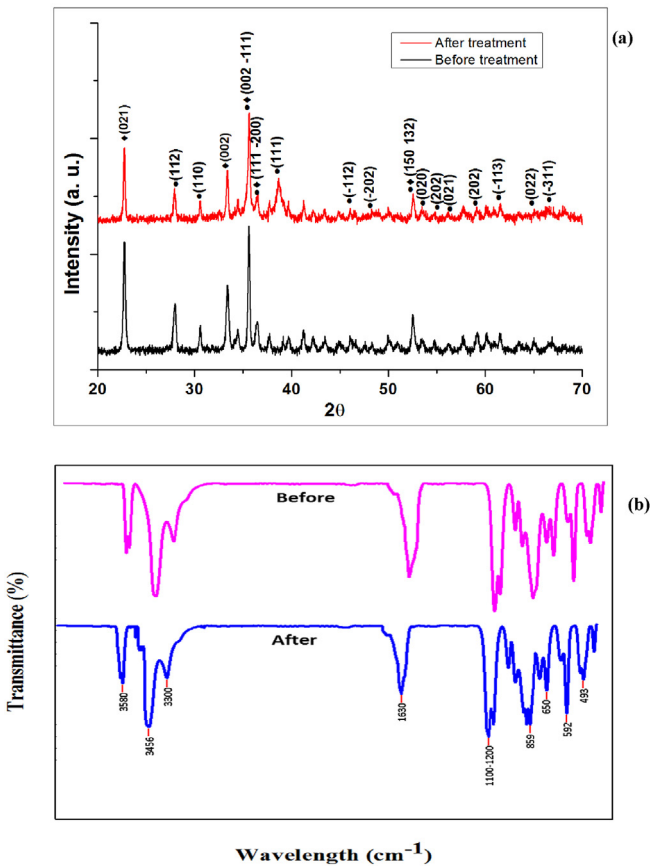

Fig. 1. (a) XRD diffractogram and (b) FTIR spectrum of the synthesized CuONs before and after photocatalytic treatment.

crystallite size of synthesized CuONs (D value) was calculated as approximately 24 nm.

FTIR measurements were carried out in order to identify the presence of various functional groups in CuONs. The FTIR spectrum of synthesized CuONs shows weak absorption peaks at 3456 and at 1630 cm^{-1}, which are ascribed with the stretching and bending vibrations related to water molecules and surface hydroxyls, respectively, that are chemically associated with CuO (Fig. 1b). A peak at 3300 cm^{-1} corresponds to C–H bond stretching, whereas the stretching of carbonyl C=O bonds results in a peak at 1100-1200 cm^{-1}. The obtained strong absorption peaks at 493, 592, and 600 cm^{-1} (in the 490-800 cm^{-1} spectrum) confirmed the typical monoclinic phase of pure CuO (Fig. 1b). The metal–oxygen (M–O) stretching in CuO can be seen at 650 cm^{-1}, which is considered as a characteristic band of the monoclinic phase of CuO. The results are similar to those in previous reports (Dhineshbabu et al., 2016; Gandhi et al., 2010).

3.2. Morphological and elemental analysis of synthesized CuONs

The most important factors that influence catalytic activity are the structure and morphology of the photocatalyst. The surface morphological study of chemically synthesized CuO/$Cu(OH)_2$ films was carried out using FE-SEM. Fig. 2a depicting the FE-SEM micrograph of CuO/$Cu(OH)_2$ nanostructures show interconnected nanopetal- or nanorod-like morphology all over the surface area of the sample having grain sizes varying from 36 to 250 nm. Such a type of compact morphology indicates a high surface area that offers the structural basis for the high surface performance. Significantly, a highly compact nanostructure is a potential candidate for photocatalytic degradation as well as various biological applications requiring antibacterial and antioxidant properties. Fig. 2b shows the EDX spectrum of the synthesized CuONs where the peaks are related to the chemical composition of both copper, oxygen and the other minor peaks of the substrate, made of Si, C and Au. No other elements was detected, excluding the presence of CuO or $Cu(OH)_2$. The EDX spectrum analysis shows the conformation of Cu and O states in all of the CuONs samples. The Cu:O atomic ratio was observed to be 2:1, confirming the presence of CuO and $Cu(OH)_2$, which can be concluded from XRD pattern.

HR-TEM analysis demonstrated that synthesized CuONs exhibited an approximate equiaxed shape with no sharp edges observed, as shown in Fig. 2c. The representative HR-TEM image of the CuONs shows a lattice fringe with a regular spacing of 0.253 nm (along the *c*-axis), which further confirms these particles are single crystals, uniformly shape, and dislocation free. The average particle sizes obtained from TEM images were 22.40 ± 1.61 nm for CuONs (Fig. 2c) and found to be very near to the crystallite size measured using the XRD results, which proves the results of TEM are in well agreement as that of the XRD results. The SAED pattern (Fig. 2d) taken of the platelet exhibits the crystalline structure of CuONs, which also correlates with the XRD results presented above. Similar

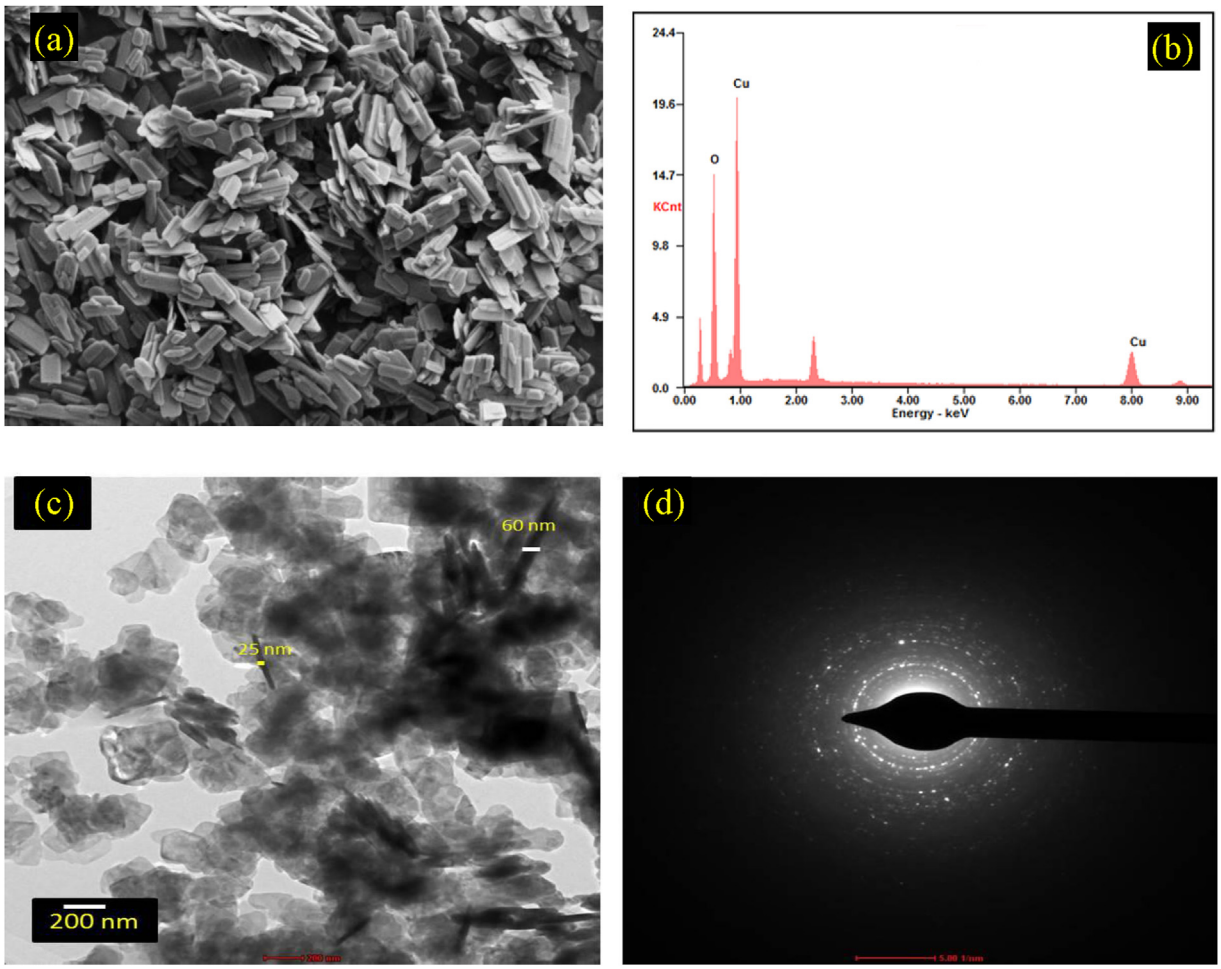

Fig. 2. (a) FE-SEM, (b) EDX, (c) HR-TEM and (d) SAED pattern of the synthesized CuONs.

Please cite this article in press as: Saratale, R.G., et al., Photocatalytic activity of CuO/$Cu(OH)_2$ nanostructures in the degradation of Reactive Green 19A and textile effluent, phytotoxicity studies and their biogenic properties (antibacterial and anticancer), Journal of Environmental Management (2018), https://doi.org/10.1016/j.jenvman.2018.04.072

results were obtained in a previous study of CuO nanocrystals synthesized on copper foil through a mild hydrothermal process (Liu et al., 2006).

3.3. Photocatalytic degradation of RG19A using the synthesized CuONs

C.I. Reactive Green 19A being toxic, sulfonated azo dye and pose health risks, thus the removal of dye and its further complete degradation leads to a growing frame of research. (Fig. 3a). Photocatalytic degradation has proved to be an efficient tool for the destruction of broad range of organic contaminants with higher mineralization (Navaee and Salimi, 2017; Kou et al., 2017). Both the photocatalyst (CuONs) and a light source are important to ensure the photocatalysis reaction in effective manner. In the case of the synthesized CuONs, almost complete degradation of RG19A was achieved (98%) within 12 h of incubation which shows that it is a very efficient photocatalyst in RG19A dye degradation. Up to 6 h of incubation the dye degradation efficiency was found higher however, further increase in incubation no significant difference in the degradation efficiency was observed and thus this time could be considered as optimum contact time.

In the preliminary investigation, three experiments were carried out: (i) irradiation of RG19A with UV light, (ii) CuONs with UV light irradiation, and (iii) CuONs without light irradiation, as shown in Fig. 3b. There was very slight degradation (0.5%) was observed when the reaction in the presence of UV light without a catalyst occurred. There was no degradation noticed in the existence of UV light. In addition, less than approximately 5% decrease in dye concentration took place in case of the experiment performed with CuONs in the absence of UV light this might be due to the adsorption whereas with CuONs in the presence of UV light irradiation, complete photocatalytic degradation of RG19A was recorded. From this, it is clear that UV light and the photocatalyst are indispensable for the enhanced degradation of RG19A dye. It was found that the color of the catalyst before and after use was the same which was confirmed by FTIR and XRD analysis in which there is no change in peaks in FTIR spectrum was recorded however reduction in the intensity of XRD diffractogram was observed in repeatedly used sample. These results suggest that the photocatalyst is stable and also reveals that the adsorbed RG19A had been completely degraded. Similar performance was seen in case of the photocatalytic degradation of Trypan Blue and Methyl Orange azo dyes by cerium-loaded CuO nanoparticles (Sasikala et al., 2016).

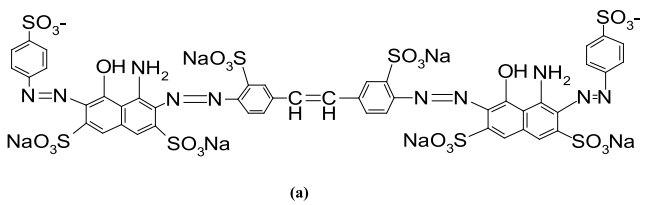

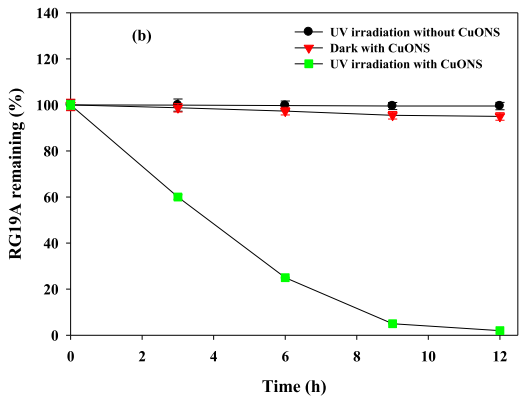

Fig. 3. (a) The chemical structure and information about Reactive Green 19A (RG19A) dye common name: Green HE4BD, CAS No.: 61931-49-5, λ_{max} (nm): 640 tested in this study, (b) The effect of various conditions on the photocatalytic degradation performance of CuONs (200 mg/L) on RG19A (50 mg/L).

3.4. Time course degradation of RG19A and its UV–vis spectra

UV visible spectroscopy can be considered one of the essential tool to understand the degradation performance of textile dyes or colorants. Fig. 4 shows the changes in the extinction spectra of RG19A taken at different time intervals during the photocatalytic degradation and observed in the wavelength region between 300 and 800 nm. During time course degradation absorption spectra showed a decrease in absorption peak intensity at 600 nm, confirming the degradation of RG19A, as shown in Fig. 4. Noticeable changes occurred in the absorbance spectra of RG19A recorded at regular time intervals under UV light irradiation with the CuONs photocatalyst. During the time course of the degradation experiments, the dye RG19A decolorized and degraded due to decomposition (photoelectrochemical oxidation). The absorbance at 200–800 nm endorsed the $\pi \rightarrow \pi^*$ transition of the aromatic part of azo dyes, the reason for the color of azo dyes and the decrease in absorbance is mainly because of the degradation of aromatic ring present in the dye (Subash et al., 2014). Upon increased reaction time, all of the absorbance peaks of the dye molecules decreased steadily and no new peaks are shown during irradiation in the analyzed wavelength range. This denoted the main chromophoric group and aromatic part in the original dye solution were devastated in the presence of CuONs under UV light illumination. Similar result was observed in the photocatalytic degradation of Metanil Yellow (an azo dye) using UV-TiO_2 and Trypan Blue and Methyl Orange by cerium loaded CuO nanoparticles (Sasikala et al., 2016; Sleiman et al., 2007).

For more details of photocatalytic activity of CuONs sample, we have calculated band gap energy of synthesized CuONS sample using following classical relation.

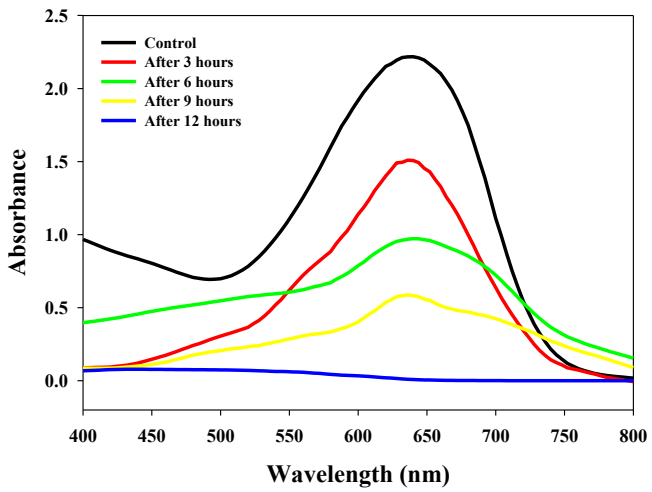

Fig. 4. Uv–vis spectra of the photocatalytic degradation of RG19A (50 mg/L) using CuONs (200 mg/L) over different time intervals.

Please cite this article in press as: Saratale, R.G., et al., Photocatalytic activity of CuO/$Cu(OH)_2$ nanostructures in the degradation of Reactive Green 19A and textile effluent, phytotoxicity studies and their biogenic properties (antibacterial and anticancer), Journal of Environmental Management (2018), https://doi.org/10.1016/j.jenvman.2018.04.072

$$\alpha = \frac{A(h\nu - E_g)^{n/2}}{h\nu}$$

where, α is the absorption coefficient, A is proportionality constant, h is the Plank's constant, υ is the light frequency of photon, Eg is the band gap energy, n depends on the nature of transition in a semiconductor (n = 1 for direct or indirect n = 4 transition) materials.

Fig. S1 shows the optical absorption spectrum of CuONs ranging from ultraviolet to visible regions (200–800 nm). A sharp absorbance peak at 298 nm could be attributed to the plasmon resonance absorption of CuO nanostructures. Fig. S1 inset shows a plot of intercepts of the tangents to the $(\alpha h\upsilon)^2$ versus photon energy ($h\upsilon$) for the determination of the band gap. This plot was found a linear at the absorption edge, confirming that the material has a direct band gap, extrapolation of straight line to the energy axis for zero absorption coefficient value gives the optical band gap emulsion. The optical absorbance with wavelength confirmed that the CuONs is semiconducting material with band gap (Eg) energy which was found to be 2.39 eV. This calculated value of band gap energy is in accordance with the reported literature (Rayapa Reddy, 2017).

Chemical oxygen demand (COD) and total organic carbon is a significant factor for evaluating the concentration of untreated organic components present in wastewater. The mineralization of RG19A was evaluated by measuring the COD and TOC content at different time intervals of illuminated solution applying appropriate UV light environment. About 84% of COD and 80% of TOC reduction was observed after 12 h of photocatalytic degradation by CuONs (data not shown). The TOC and COD results clearly point out the complete breakdown of dye molecules into CO_2 and H_2O resulting in significant mineralization.

3.5. Optimization of various physicochemical conditions

In the photocatalytic degradation of dyes process mainly based on several parameters like the type and the concentration of the organic compound, source of light, and light intensity, pH, and temperature (Akpan and Hameed, 2009). The decolorization performance of the CuONs (200 mg/L) on RG19A was carried out by using different dye concentrations (50–250 mg/L). It was observed that with the increasing concentrations of dye, the rate of degradation performance decreased (Fig. 5a). Dye concentrations of 50, 100, and 150 mg/L achieved about 100, 98, and 92% of degradation at 8, 12, and 18 h, respectively. However, when the dye concentration was 200 mg/L, only 70% degradation was noticed after 24 h. The percentage of degradation declined sharply at dye concentrations greater than 250 mg/L, where only 40% degradation was achieved at 24 h of incubation. Additionally, the photocatalytic degradation performance having concentration of dye at 100 mg/L was performed using various CuONs concentrations. Complete degradation at different CuONs concentrations (100, 200, 300, 400, and 500 mg/L) was achieved after 20, 12, 8, 6, and 5 h, respectively (Fig. 5b). These results proved that the photocatalytic degradation rate increases with an increase in concentration of CuONs. The cause behind this is that increased loading of CuONs leads to increase the number of total active sites on the surface of the photocatalyst which enhances absorption of photons and hence generation of more hydroxyl radicals. However, above the optimum value, the degradation rate decreases this might be owing to the interception of the light by the suspension, aggregation of the catalyst particles and scattering effects, and reduction in the penetration of photons (Esmaili-Hafshejani and Nezamzadeh-Ejhieh, 2016; Nezamzadeh-Ejhieh and Ghanbari-Mobarakeh, 2015; Chakrabarti and Dutta, 2004). The present investigation revealed that CuONs induced photoelectrocatalysis of RG19A

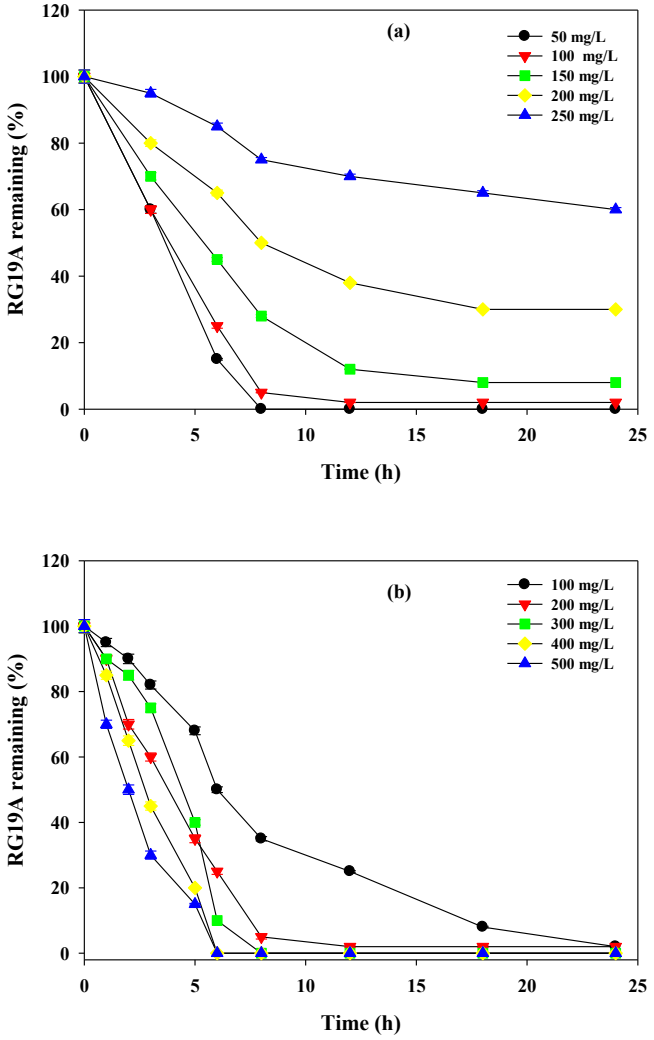

Fig. 5. The photocatalytic degradation of RG19A (50–250 mg/L) using synthesized CuONs (200 mg/L), and (B) different CuONs concentrations (100–500 mg/L) for the degradation of RG19A (100 mg/L).

follows the first order kinetics derived from the first order plots (Table S1) which is similar to earlier reports (Naghizade Asl et al., 2016) The photodegradation rate constants (based on the slopes of the corresponding curves) are presented in Table S1.

3.6. Reusability and stability of the CuONs during the photocatalytic degradation of RG19A

Generally, the life span of a photocatalyst is a vital factor during the photocatalytic degradation of organic pollutants. Concerning this, we determined the stability of CuONs for the photocatalytic degradation of RG19A. We checked the catalyst's lifetime for its reusability by performing the degradation experiment with the collected photocatalyst continually over four cycles. CuONs revealed significant photostability without any substantial loss in photocatalytic activity even up to the fourth cycle. The foregoing results point out that CuONs catalyst found more effective and reusable under UV light. There was no major loss of photocatalytic activity up to four runs (98, 98, 95.4% and 90.0%, respectively), but after the third cycle, an increase in the incubation period was required for better degradation of RG19A (Fig. 6). The significant TOC (79%) and COD (75%) removal at the end of the fourth cycle was

Please cite this article in press as: Saratale, R.G., et al., Photocatalytic activity of CuO/Cu(OH)$_2$ nanostructures in the degradation of Reactive Green 19A and textile effluent, phytotoxicity studies and their biogenic properties (antibacterial and anticancer), Journal of Environmental Management (2018), https://doi.org/10.1016/j.jenvman.2018.04.072

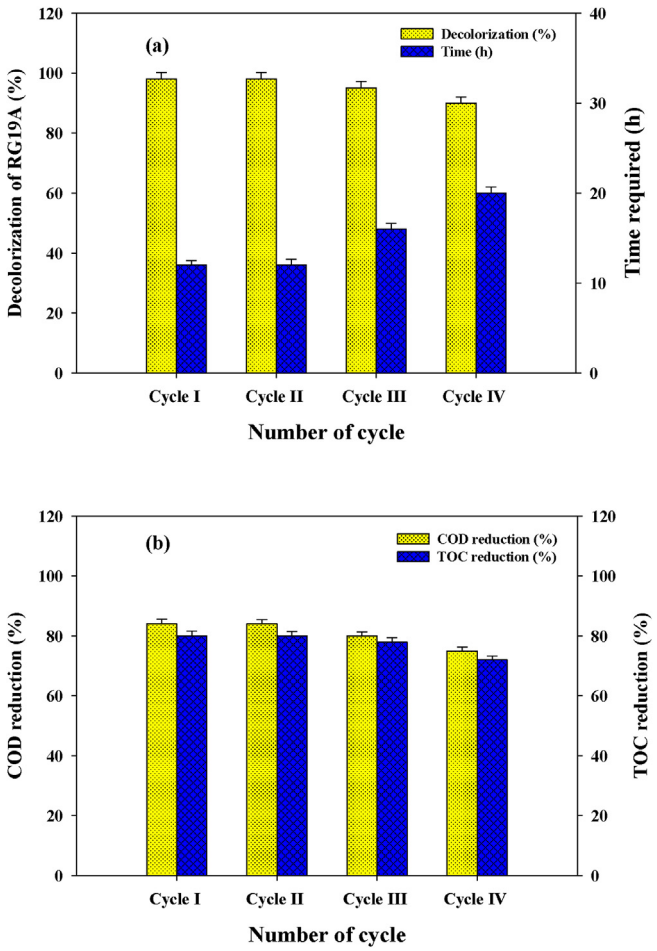

Fig. 6. Determination of the reusability of synthesized CuONs for the photocatalytic degradation of (A) RG19A dye (50 mg/L), and (B) TOC and COD reduction at different repeated use cycles.

also observed after repeated use of the photocatalyst, which further increases the value of the study (Fig. 6). However, at the fourth cycle, the photocatalytic degradation performance decreased (55%) after 24 h of incubation (data not shown). This could be because of lack of appropriate electron-hole scavengers of CuONs, resulting in less degradation of the dye.

The color of the recovered photocatalyst was the same as that when newly prepared, which indicates that it is stable during the photocatalytic reaction. We have performed FTIR and XRD analysis of the photocatalyst before and after reuse in which the there is no change in peaks in FTIR was observed however reduction in the peak intensity of XRD diffractogram was noticed (Fig. 1a and b). The foregoing results suggest that the photocatalyst is stable and also reveals that the adsorbed RG19A had been completely degraded. These results also validate the applicability of implementing this technology in practical wastewater treatment.

3.7. Mechanism of dye degradation

Photocatalytic degradation (irradiated with UV light), results to form electron/hole (e^-/h^+) pairs with free electrons generated from the valence band (VB) to the conduction band (CB), and thus departing a hole in the valence band (Eq. (2)) (Chen and Ray, 1998). The amount of electron-hole pairs in a photocatalyst mainly based on the intensity of the incidental light and as well the electronic characteristics of the materials. In the photocatalytic process, if separation of charge is sustained, this allows the electrons and hole to travel towards the catalyst's surface where they involve in redox reactions with adsorbed species. Particularly, h_V may interact to surface-bound H_2O or OH^- to generate the hydroxyl radical ($OH^•$) and oxygen forming superoxide radical anion ($O^{•-}_2$) (Eqs. (3)–(5)). We suppose that the highly reactive $O_2^{•-}$ and $OH^•$ were used in the degradation process of RG19A dye molecules using the CuONs photocatalyst (Eqs. (2)–(7)) (Azimi and Nezamzadeh-Ejhieh, 2015; Wu et al., 2010; Subash et al., 2014). However, with a lack of appropriate electron-hole scavengers, the photogenerated electron-hole pairs may have recombined and scattered the input energy in form of heat within a few nanoseconds. Hence, the electron acceptors are necessary for the efficient photocatalytic process (Fig. 7):

$$\mathrm{CuONs} + h\nu \rightarrow \mathrm{CuONs}\left(e_{cb}^- + h_{vb}^+\right), \quad (2)$$

$$O_2 + e_{cb}^- \longrightarrow O_2^{•-}, \quad (3)$$

$$h_{vb}^+ + H_2O \longrightarrow OH^• + H^+, \quad (4)$$

$$h_{vb}^+ + OH^- \longrightarrow OH^•, \quad (5)$$

$$O_2^{•-} + \text{dye} \longrightarrow \text{dye products}, \quad (6)$$

$$OH^• + \text{dye} \longrightarrow \text{dye products}. \quad (7)$$

In this work, $CuO/Cu(OH)_2$ nanostructures along with the surface area and the surface hydroxyl groups (−OH•) of $Cu(OH)_2$ take an important role in the photocatalytic process by accepting photogenerated holes to form hydroxyl radicals (-OH•) thus preventing electron-hole recombination in $CuO/Cu(OH)_2$ photocatalysts (Akhavan et al., 2011; Wang et al., 2015). The OH• radicals can be produced through interaction of the photoexcited hole of the CuO with the surface OH bonds of $Cu(OH)_2$, and thus may act as the source of OH• which can be considered as one of the important parameters in degradation. Another important reason for such a high activity can be attributed to the interface between $Cu(OH)_2$ and CuO, near which the higher valence sites Cu(II)) in the hydroxide layer may increase the trapping of the photogenerated electrons (Wang et al., 2015). Thus, the $CuO/Cu(OH)_2$ photocatalysts have the best photocatalytic activity because of the formation of excess superoxides and/or hydroxyl radicals on the surface of $CuO/Cu(OH)_2$ photocatalysts.

3.8. Photocatalytic degradation of actual textile wastewater by CuONs

Usually all the industrial dyes have highly complex and varied chemical constituents and they are selected based on the type of material to be dyed. This results to vary in the color as well as chemical composition of dyeing effluent. However, a considerable decline in color removal (80% in terms of ADMI) of textile effluent was observed after photocatalytic degradation using synthesized CuONs within 24 h of incubation. Moreover, there was a significant decrease in COD (72%) and TOC (69%), which indicates significant mineralization of the textile effluent after photocatalytic treatment (Table 1). The foregoing results indicate the practical applicability of CuONs in textile wastewater treatment.

3.9. Phytotoxicity studies of RG19A, textile effluent, and metabolites after photocatalytic degradation

Discharge of dyeing effluents without treatment in water

Please cite this article in press as: Saratale, R.G., et al., Photocatalytic activity of $CuO/Cu(OH)_2$ nanostructures in the degradation of Reactive Green 19A and textile effluent, phytotoxicity studies and their biogenic properties (antibacterial and anticancer), Journal of Environmental Management (2018), https://doi.org/10.1016/j.jenvman.2018.04.072

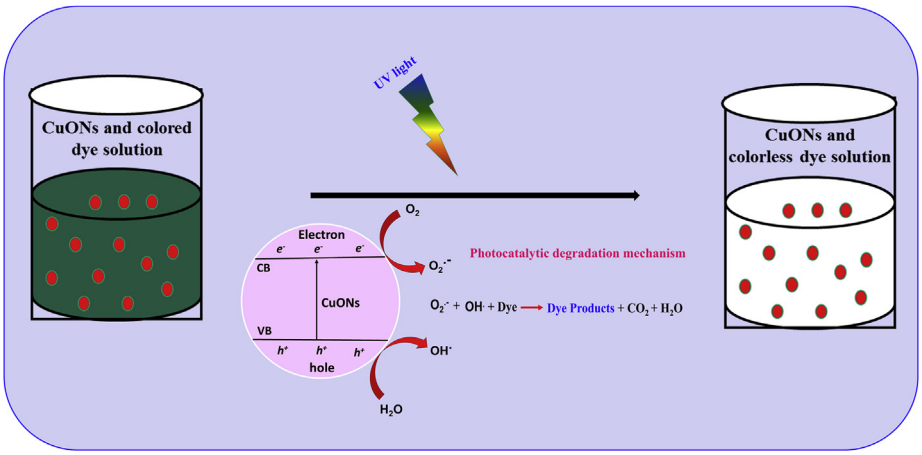

Fig. 7. Proposed mechanism for photocatalytic degradation of RG19A by CuO nanostructures.

Table 1
Photocatalytic degradation of textile effluent (diluted 1:1) using synthesized CuONs (200 mg/L) and its TOC and COD reduction over different time intervals.

Time (h)	Decolorization in terms of ADMI (%)	COD reduction (%)	TOC reduction (%)
0	0.0[a]	0.0[a]	0.0[a]
6	22 ± 0.85[b]	12.5 ± 0.45[b]	11.2 ± 0.24[b]
12	54 ± 1.45[c]	42.8 ± 0.89[c]	39.6 ± 0.95[c]
18	72 ± 1.58[d]	65.6 ± 1.15[d]	62.5 ± 1.24[d]
24	80 ± 2.15[e]	72.0 ± 1.45[e]	69.2 ± 1.34[e]

Means are followed by standard errors. Within a column, different letters indicate significant differences (ANOVA followed by Tukey's HSD test).

streams might pose serious threat to ecosystem and health risks to human being (Saratale et al., 2011). Concerning this, we assessed the phytotoxicity of RG19A and actual textile effluent before and after photocatalytic degradation. The phytotoxicity study of the RG19A, actual textile effluent, and their products after photocatalytic degradation are presented in Table 2. Results of the phytotoxicity carried out using *P. mungo* and *S. vulgare* confirmed the degradation products of RG19A and effluent showed no inhibition in the germination of plant seeds and almost showed similar performance in case of germination rate, plumule length and radicle length with those treated with distilled water only (Table 2). The germination rate as well as plumule and radicle length of *P. mungo* and *S. vulgare* were extremely affected when exposed to RG19A and textile effluent (each 400 ppm) compared to degraded products set. The phytotoxicity studies discovered that the products generated after photocatalytic degradation of RG19A and textile effluent were less toxic in nature (Table 2). In the case of *P. mungo* and *S. vulgare* growth, the mean of plumule lengths (cm) were 12.0 and 10.24, respectively, when watered with distilled water (D/W on the table) whereas when exposed to RG19A, they were 6.45 and 5.62, respectively, and with its extracted metabolites, grew to approximately 9.05 and 9.42, respectively. Similarly, shoot length of both plant species, showed a drastic effect when they were exposed to RG19A as compared to their extracted metabolites after photocatalytic treatment. In the case of *S. vulgare seeds* exposed to RG19A dye and its extracted metabolites, the germination rates were about 60 and 90%, respectively, whereas seeds exposed to effluent and its extracted metabolites showed germination rates of 40% and 80%, respectively. Moreover, when both plant species were exposed to actual industrial effluent, it directly affected seed germination as well as radicle and plumule length, but after photocatalytic treatment, plants treated with the metabolites showed increased growth over those exposed to pretreated effluent in all studied parameters (Table 2). The results suggest that using CuONs photocatalytic degradation of dye containing effluent is safe, which in turn enhancing its feasible use in real applications.

Table 2
Phytotoxicity studies of RG19A, actual textile effluent, and its metabolites formed after photocatalytic degradation using synthesized CuONs (200 mg/L) on *Phaseolus mungo* and *Sorghum vulgare*.

Parameter	Control		RG19A				Textile effluent			
	Phaseolus mungo	*Sorghum vulgare*	*Phaseolus mungo*		*Sorghum vulgare*		*Phaseolus mungo*		*Sorghum vulgare*	
	D/W	D/W	RG19A[a]	EM[a]	RG19A[a]	EM[a]	Effluent[a]	EM[a]	Effluent[a]	EM[a]
Germination (%)	100	100	70*	100	60*	90	50*	90	40*	80*
Plumule (cm)	12.00 ± 0.88	10.24 ± 0.78	6.45 ± 0.34*	9.05 ± 0.65	5.62 ± 0.35*	9.42 ± 0.62	4.12 ± 0.32*	8.65 ± 0.88	3.24 ± 0.39*	8.12 ± 0.68
Radical (cm)	3.24 ± 0.25	4.85 ± 0.44	1.42 ± 0.31*	2.54 ± 0.32*	1.70 ± 0.24	3.42 ± 0.39	1.18 ± 0.26*	3.65 ± 0.41	1.35 ± 0.11*	2.84 ± 0.31*

RG19A: Reactive Green 19A; D/W: distilled water; EM: extracted products of dye and effluent after photocatalytic degradation.
Values are mean of three replicates, followed by standard errors. Asterisks indicated significant differences from the control (seeds germinated in water) at *P < 0.05 (ANOVA followed by Tukey's HSD test).
[a] 400 ppm concentration.

Please cite this article in press as: Saratale, R.G., et al., Photocatalytic activity of CuO/$Cu(OH)_2$ nanostructures in the degradation of Reactive Green 19A and textile effluent, phytotoxicity studies and their biogenic properties (antibacterial and anticancer), Journal of Environmental Management (2018), https://doi.org/10.1016/j.jenvman.2018.04.072

3.10. Biogenic properties of synthesized of CuONs

3.10.1. Antibacterial activity

The synthesized CuONs exhibited significant antibacterial activity against human pathogens in terms of zone of inhibition (ZOI). In the preliminary investigation, we checked that the antibacterial potential of CuONs showed maximum ZOI with both selected microorganism: *E. coli* (16 mm) and *S. aureus* (13.5 mm) (data not shown). The variation in the ZOI could be due to the differences present in the cell wall composition among Gram-positive and Gram-negative bacteria. For CuONs impregnated with antibiotics, vancomycin showed a particularly enhanced ZOI diameter whereas a moderate increase in ZOI was observed in the case of amoxicillin for both tested bacteria (Table 3). However, in the case of CuONs with oxy-tetracycline, a more enhanced ZOI in *E. coli* compared to *S. aureus* was observed (Table 3). This enhanced antibacterial activity reveals the prominent application of CuONs in the field of development of antibacterial drugs to kill pathogenic bacteria. Photographs of plates loaded with the above selected antibiotics and CuONs impregnated with antibiotics are shown in Fig. S2.

3.10.2. Antioxidant activity

The antioxidant activity of the synthesized CuONs was determined using DPPH and ABTS radical scavenging activity assays and the obtained results are exhibited in Fig. 8. Both the radical scavenging activity of CuONs increased with increased concentration and was found to have a dose-dependent nature with respective IC_{50} values of 60 μg/mL and 51 μg/mL (Fig. 8) related to the standard IC_{50} value 45 μg/mL for catechol and IC_{50} value 36.4 μg/mL for standard ascorbic acid. Percent inhibition of DPPH and ABTS radical scavenging activity was illustrated in Fig. 8a and b. The increased DPPH and ABTS radical scavenging potential could be because of the ability of CuONs that tends to donate electrons or hydrogen ions. The antibacterial and antioxidant potential of the CuONs could be useful in the development of antibacterial drugs against certain pathogenic bacteria.

3.10.3. In vitro cytotoxicity assessment

We have assessed the anticancer potential of CuONs against tumor rat C6 cell line with a different initial concentrations (10–100 μg/mL). The results from this study reveals, the direct dose dependent performance with the C6 cells at increased concentrations. In this study a minimum of 60 μg/mL of CuONs is sufficient to induce 50% of cell mortality whereas standard drug Doxorubocin was supplemented at 25 μg/mL inhibiting about 40% of cancer cells growth. In contrast, the presence of 100 μg/mL of CuONs showed almost complete inhibition of the cell growth (>95%) (Fig. 9). It was supposed that CuONs show anticancer potential through their free radicals scavenging ability that results in cellular destruction and eventually in cell death. Nonetheless, this is the first time report on cytotoxic potential of CuONs against cancer cells (C6 cell line) however, more detailed research is required to understand the particular mechanism involved in the anticancer study.

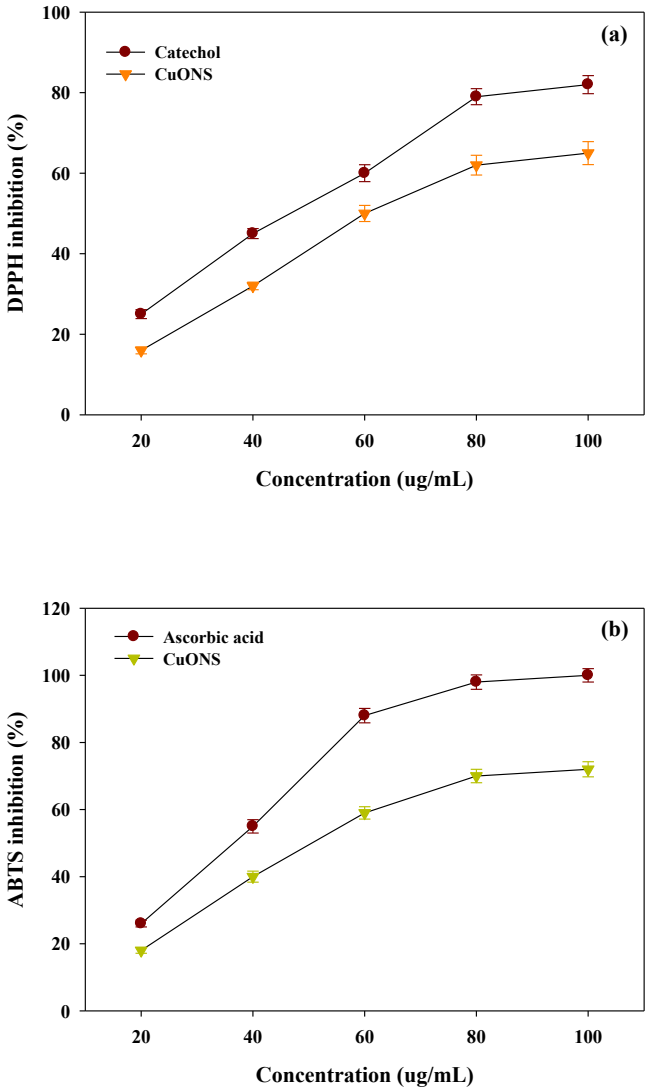

Fig. 8. Antioxidant activity in terms of (a) DPPH (2,2-diphenylamine-1-picryl hydrazyl) and (b) ABTS (2,2′-azino-bis(3-ethylbenzothiazoline-6-sulphonic acid)) radical scavenging activity of the synthesized CuONs.

4. Conclusions

In the present investigation, the $CuO/Cu(OH)_2$ nanostructures were successfully prepared via a simple chemical route and were characterized using various analytical tools. The photocatalytic activity of CuONs was investigated by photocatalytic degradation of

Table 3
Enhanced antibacterial activity of synthesized CuO nanostructures on human pathogens *Escherichia coli* and *Staphylococcus aureus*.

Antibiotic (μg)	*Escherichia coli*			*Staphylococcus aureus*		
	ZOI (mm)			ZOI (mm)		
	Ab	Ab + CuONs	Enhanced ZOI (%)	Ab	Ab + CuONs	Enhanced ZOI (%)
Vancomycin (30)	15.0 ± 0.48^{a}	24.2 ± 0.52^{a}	61.3	18.0 ± 0.48^{a}	24.2 ± 0.52^{a}	34.4
Oxytetracycline (30)	25.1 ± 0.54^{b}	30.2 ± 0.48^{b}	20.3	32.0 ± 0.62^{c}	33.2 ± 0.64^{b}	3.80
Amoxicillin + Clavulanic acid (20 + 10)	26.0 ± 0.44^{b}	29.1 ± 0.48^{b}	11.9	26.0 ± 0.49^{b}	31.2 ± 0.54^{b}	20.0

ZOI = zone of inhibition; Ab = antibiotic; CuONs = Copper oxide nanostructures.
Values are means of three replicates ± standard errors. Within a column, different letters indicate significant differences (ANOVA followed by Tukey's HSD test).

Please cite this article in press as: Saratale, R.G., et al., Photocatalytic activity of $CuO/Cu(OH)_2$ nanostructures in the degradation of Reactive Green 19A and textile effluent, phytotoxicity studies and their biogenic properties (antibacterial and anticancer), Journal of Environmental Management (2018), https://doi.org/10.1016/j.jenvman.2018.04.072

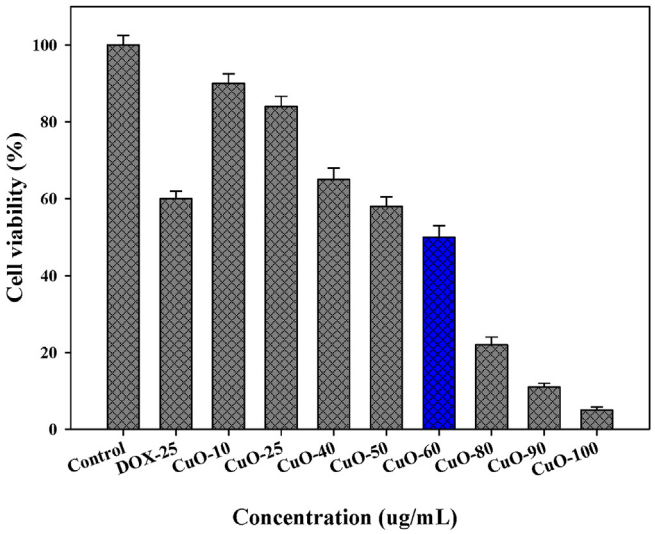

Fig. 9. Anticancer activity of synthesized CuONs against C6 neural rat glial tumor cell lines at different concentrations. The *blue column* in figure indicates IC_{50} value of CuONs against rat glial tumor C6 cells. Doxorubocin (*DOX-25)* at a concentration of 25 μg/mL. (For interpretation of the references to color in this figure legend, the reader is referred to the Web version of this article.)

RG19A dye and actual textile effluent under UV light illumination at room temperature. The obtained results showed significant degradation of RG19A and actual textile effluent with higher removal of TOC and COD. Phytotoxicity study of the degraded metabolites of RG19A and effluent after photocatalytic treatment were less toxic in nature. The developed photocatalytic process using CuONs showed promising efficiency and could possibly be applied in the remediation of actual textile effluents due to the advantages of its simplicity, being low-priced and stable, reusability, and tremendous performance. Lastly, the maximum scavenging efficacy of CuONs in terms of antioxidant activity, and the antibacterial activity of synthesized CuONs were evaluated. Anticancer activity against rat tumor C6 cell line also increases the potential application of synthesized CuONs in various biomedical applications.

Conflict of interest

The authors declare that no conflicting interests exist.

Acknowledgements

This research was completely supported by Dongguk University-Seoul, South Korea under research fund 2016–2018. Authors are thankful to Mr. Oh Sin-Taek, Dongguk University for his technical help during the cytotoxicity studies and Dr. Mahadeo Mahadik from Chonbuk National University, South Korea for his technical help during revision. Thanks to Prof. Shrikrishna D. Sartale, Department of Physics, Savitribai Phule Pune University, India, for availing HRTEM facility.

Appendix A. Supplementary data

Supplementary data related to this article can be found at https://doi.org/10.1016/j.jenvman.2018.04.072.

References

Akhavan, O., Azimirad, R., Safa, S., Hasani, E., 2011. $CuO/Cu(OH)_2$ hierarchical nanostructures as bactericidal photocatalysts. J. Mat. Chem. 21, 9634–9640.

Akpan, U.G., Hameed, B.H., 2009. Parameters affecting the photocatalytic degradation of dyes using TiO_2-based photocatalysts: a review. J. Hazard. Mater. 170, 520–529.

Amani-Beni, Z., Nezamzadeh-Ejhieh, A., 2017. A novel non-enzymatic glucose sensor based on the modification of carbon paste electrode with CuO nanoflower: designing the experiments by response surface methodology (RSM). J. Colloid Interface Sci. 504, 186–196.

American Public Health Association, American Water Works Association, Water Environment Federation, 1998. Standard Methods for the Examination of Water and Wastewater, twentieth ed. National Government publication, Washington, DC.

Azimi, S., Nezamzadeh-Ejhieh, A., 2015. Enhanced activity of clinoptilolite-supported hybridized PbS–CdS semiconductors for the photocatalytic degradation of a mixture of tetracycline and cephalexin aqueous solution. J. Mol. Catal. 408, 152–160.

Bedekar, P.A., Saratale, R.G., Saratale, G.D., Govindwar, S.P., 2014. Oxidative stress response in dye degrading bacterium *Lysinibacillus* sp. RGS exposed to Reactive Orange 16, degradation of RO16 and evaluation of toxicity. Environ. Sci. Pollut. Res. 21, 11075–11085.

Buthiyappan, A., Aziz, A.R.A., Daud, W.M.A.W., 2016. Recent advances and prospects of catalytic advanced oxidation process in treating textile effluents. Rev. Chem. Eng. 32, 1–47.

Chakrabarti, S., Dutta, B.K., 2004. Photocatalytic degradation of model textile dyes in wastewater using ZnO as semiconductor catalyst. J. Hazard. Mater. 112, 269–278.

Chen, D., Ray, A.K., 1998. Photodegradation kinetics of 4-nitrophenol in TiO2 suspension. Water Res. 32, 3223–3234.

Choi, K.J., Jang, H.W., 2010. One-dimensional oxide nanostructures as gas-sensing materials: review and issues. Sensors 10, 4083–4099.

Derikvandi, H., Nezamzadeh-Ejhieh, A., 2017. Increased photocatalytic activity of NiO and ZnO in photodegradation of a model drug aqueous solution: effect of coupling, supporting, particles size and calcination temperature. J. Hazard. Mater. 321, 629–638.

Dhineshbabu, N.R., Rajendran, V., Nithyavathy, N., Vetumperumal, R., 2016. Study of structural and optical properties of cupric oxide nanoparticles. Appl. Nanosci. 6, 933–939.

Esmaili-Hafshejani, J., Nezamzadeh-Ejhieh, A., 2016. Increased photocatalytic activity of Zn(II)/Cu(II) oxides and sulfides by coupling and supporting them onto clinoptilolite nanoparticles in the degradation of benzophenone aqueous solution. J. Hazard. Mater. 316, 194–203.

Filipič, G., Cvelbar, U., 2012. Copper oxide nanowires: a review of growth. Nanotechnology 23, 194001.

Gandhi, S., Subramani, R.H.H., Ramakrishnan, T., Sivabalan, A., Dhanalakshmi, V., Nair, M.R.G., Anbarasan, R., 2010. Ultrasound assisted one pot synthesis of nanosized CuO and its nanocomposite with poly(vinyl alcohol). J. Mat. Sci. 45, 1688–1694.

Gaya, U.I., Abdullah, A.H., 2008. Heterogeneous photocatalytic degradation of organic contaminants over titanium dioxide: a review of fundamentals, progress and problems. J. Photochem. Photobiol. C. Photochem. Rev. 9, 1–12.

Houas, A., Lachheb, H., Ksibi, M., Elaloui, E., Guillard, C., Herrmann, J.-M., 2001. Photocatalytic degradation pathway of methylene blue in water. Appl. Catal. B Environ. 31, 145–157.

Katwal, R., Kaur, H., Sharma, G., Naushad, M., Pathania, D., 2015. Electrochemical synthesized copper oxide nanoparticles for enhanced photocatalytic and antimicrobial activity. J. Ind. Eng. Chem. 31, 173–184.

Kou, J., Lu, C., Wang, J., Chen, Y., Xu, Z., Varma, R.S., 2017. Selectivity enhancement in heterogeneous photocatalytic transformations. Chem. Rev. 117, 1445–1514.

Liu, Y., Chu, Y., Li, M., Li, L., Dong, L., 2006. In situ synthesis and assembly of copper oxide nanocrystals on copper foil via a mild hydrothermal process. J. Mat. Chem. 16, 192–198.

Maleki, A., Safari, M., Shahmoradi, B., Zandsalimi, Y., Daraei, H., Gharibi, F., 2015. Photocatalytic degradation of humic substances in aqueous solution using Cu-doped ZnO nanoparticles under natural sunlight irradiation. Environ. Sci. Pollut. Res. Int. 22, 16875–16880.

Mansouri, B., Maleki, A., Johari, S.A., Shahmoradi, B., Mohammadi, E., Davari, B., 2017. Histopathological effects of copper oxide nanoparticles on the gill and intestine of Common carp (*Cyprinus carpio*) in the present of titanium dioxide nanoparticles. Chem. Ecol. 33, 295–308.

Moldovan, B., David, L., Achim, M., Clichici, S., Filip, G.A., 2016. A green approach to phytomediated synthesis of silver nanoparticles using *Sambucus nigra* L. fruits extract and their antioxidant activity. J. Mol. Liq. 221, 271–278.

Naghizade Asl, M., Mahmodi, N.M., Teymouri, P., Shahmoradi, B., Rezaee, R., Maleki, A., 2016. Adsorption of organic dyes using copper oxide nanoparticles: isotherm and kinetic studies. Desal. Water Treat. 56, 25278–25287.

Navaee, A., Salimi, A., 2017. Sulfur doped-copper oxide nanoclusters synthesized through a facile electroplating process assisted by thiourea for selective photoelectrocatalytic reduction of CO_2. J. Colloid Interface Sci. 505, 241–252.

Nezamzadeh-Ejhieh, A., Ghanbari-Mobarakeh, Z., 2015. Heterogeneous photodegradation of 2,4-dichlorophenol using FeO doped onto nano-particles of zeolite P. J. Ind. Eng. Chem. 21, 668–676.

Nezamzadeh-Ejhieh, A., Hushmandrad, S., 2010. Solar photodecolorization of methylene blue by CuO/X zeolite as a heterogeneous catalyst. Appl. Catal. A 388, 149–159.

Nezamzadeh-Ejhieh, A., Salimi, Z., 2011. Solar photocatalytic degradation of o-

phenylenediamine by heterogeneous CuO/X zeolite catalyst. Desalination 280, 281–287.
Nezamzadeh-Ejhieh, A., Zabihi-Mobarakeh, H., 2014. Heterogeneous photodecolorization of mixture of methylene blue and bromophenol blue using CuO-nano-clinoptilolite. J. Ind. Eng. Chem. 20, 1421–1431.
Novotny, C., Svobodová, K., Benada, O., Kofroňová, O., Heissenberger, A., Fuchs, W., 2011. Potential of combined fungal and bacterial treatment for color removal in textile wastewater. Bioresour. Technol. 102, 879–888.
Phiwdang, K., Suphankij, S., Mekprasarta, W., Pecharapa, W., 2013. Synthesis of CuO Nanoparticles by precipitation method using different precursors. Energy Procedia 34, 740–745.
Putri, L.K., Tan, L.L., Ong, W.J., Chang, W.S., Chai, S.P., 2016. Graphene oxide: exploiting its unique properties toward visible-light-driven photocatalysis. Appl. Mat. Today 4, 9–16.
Rayapa Reddy, K., 2017. Green synthesis, morphological and optical studies of CuO nanoparticles. J. Mol. Struct. 1150, 553–557.
Rehana, D., Mahendiran, D., SenthilKumar, R., Rahiman, A.K., 2017. Evaluation of antioxidant and anticancer activity of copper oxide nanoparticles synthesized using medicinally important plant extracts. Biomed. Pharmacother. 89, 1067–1077.
Ren, G., Hu, D., Cheng, E.W.C., Vargas-Reus, M.A., Reip, P., Allaker, R.P., 2009. Characterisation of copper oxide nanoparticles for antimicrobial applications. Int. J. Antimicrob. Agents 33, 587–590.
Salehi, K., Bahmani, A., Shahmoradi, B., Pordel, M.A., Kohzadi, S., Gong, Y., Guo, H., Shivaraju, H.P., Rezaee, R., Pawar, R.R., Lee, S.-M., 2017. Response surface methodology (RSM) optimization approach for degradation of Direct Blue 71 dye using CuO–ZnO nanocomposite. Int. J. Environ. Sci. Technol. 14, 2067–2076.
Salehi, K., Daraei, H., Teymouri, P., Shahmoradi, B., Maleki, A., 2016. Cu-doped ZnO nanoparticle for removal of reactive black 5: application of artificial neural networks and multiple linear regression for modeling and optimization. Desal. Water Treat. 57, 22074–22080.
Sapkal, R.T., Shinde, S.S., Mahadik, M.A., Mohite, V.S., Waghmode, T.R., Govindwar, S.P., Bhosale, C.H., 2012. Photoelectrocatalytic decolorization and degradation of textile effluent using ZnO thin films. J. Photochem. Photobiol. B 114, 102–107.
Saratale, G.D., Saratale, R.G., Benelli, G., Kumar, G., Pugazhendhi, A., Kim, D.S., Shin, H.S., 2017. Anti-diabetic potential of silver nanoparticles synthesized with *Argyreia nervosa* leaf extract high synergistic antibacterial activity with standard antibiotics against foodborne bacteria. J. Clust. Sci. 28, 1709–1727.
Saratale, G.D., Saratale, R.G., Chang, J.S., Govindwar, S.P., 2011a. Fixed-bed decolorization of Reactive Blue 172 by *Proteus vulgaris* NCIM-2027 immobilized on *Luffa cylindrica* sponge. Int. Biodeter. Biodegr. 65, 494–503.
Saratale, R.G., Saratale, G.D., Chang, J.S., Govindwar, S.P., 2009. Decolorization and biodegradation of textile dye navy blue HER by *Trichosporon beigelii* (NCIM-3326). J. Hazard. Mater.. 166, 1421–1428.
Saratale, R.G., Saratale, G.D., Chang, J.S., Govindwar, S.P., 2011. Outlook of bacterial decolorization and degradation of azo dyes: a review. J. Taiwan. Inst. Chem. Eng. 42, 138–157.
Saratale, R.G., Shin, H.S., Kumar, G., Benelli, G., Ghodake, G.S., Jiang, Y.Y., Kim, D.S., Saratale, G.D., 2018. Exploiting fruit byproducts for eco-friendly nanosynthesis: citrus × clementina peel extract mediated fabrication of silver nanoparticles with high efficacy against microbial pathogens and rat glial tumor C6 cells. Environ. Sci. Pollut. Res. 25, 10250–10263.
Saratale, R.G., Sivapathan, S.S., Jeong, W., Kim, H.-Y., Saratale, G.D., Kim, D.-S., 2016. Preparation of activated carbons from peach stone by $H_4P_2O_7$ activation and its adsorption behavior for Acid Red 18 and dye containing wastewater. J. Environ. Sci. Health A 51, 1–10.
Sasikala, R., Karthikeyan, K., Easwaramoorthy, D., Bilal, I.M., Rani, S.K., 2016. Photocatalytic degradation of trypan blue and methyl orange azo dyes by cerium loaded CuO nanoparticles. Environ. Nanotechnol. Monit. Manag. 6, 45–53.
Sleiman, M., Vildozo, D., Ferronato, C., Chovelon, J.M., 2007. Photocatalytic degradation of azo dye Metanil Yellow: optimization and kinetic modeling using a chemometric approach. Appl. Catal. B Environ. 77, 1–11.
Subash, B., Krishnakumar, B., Swaminathan, M., Shanthi, M., 2014. ZnS–Ag–ZnO as an excellent UV-light-active photocatalyst for the degradation of AV 7, AB 1, RR 120, and RY 84 dyes: synthesis, characterization, and catalytic applications. Ind. Eng. Chem. Res. 53, 12953–12963.
Wang, S.B., Hsiao, C.H., Chang, S.J., Lam, K.T., Wen, K.H., Hung, S.C., Huang, R., 2011. A CuO nanowire infrared photodetector. Sens. Actuators A Phys. 171, 207–211.
Wang, Y., Jiang, T., Meng, D., Kong, J., Jia, H., Yu, M., 2015. Controllable fabrication of nanostructured copper compound on a Cu substrate by a one-step route. RSC Adv. 5, 16277–16283.
Wongpisutpaisan, N., Charoonsuka, P., Vittayakorn, N., Pecharapa, W., 2011. Sonochemical synthesis and characterization of copper oxide nanoparticles. Energy Procedia 9, 404–409.
Wu, Y., Zhang, J., Xiao, L., Chen, F., 2010. Properties of carbon and iron modified TiO2 photocatalyst synthesized at low temperature and photodegradation of acid orange 7 under visible light. Appl. Surf. Sci. 256, 4260–4268.
Yavari, S., Mahmodi, N.M., Teymouri, P., Shahmoradi, B., Maleki, A., 2016. Cobalt ferrite nanoparticles: preparation, characterization and anionic dye removal capability. J. Taiwan Inst. Chem. Eng. 59, 320–329.
Zhang, Q., Zhang, K., Xu, D., Yang, G., Huang, H., Nie, F., Yang, S., 2014. CuO nanostructures: synthesis, characterization, growth mechanisms, fundamental properties, and applications. Prog. Mat. Sci. 60, 208–337.
Zhang, X., Shi, W., Zhu, J., Kharistal, D., Zhao, W., Lalia, B., Yang, Q., 2011. High-power and high-energy-density flexible pseudocapacitor electrodes made from porous CuO nanobelts and single-walled carbon nanotubes. ACS Nano 5, 2013–2019.

Please cite this article in press as: Saratale, R.G., et al., Photocatalytic activity of CuO/$Cu(OH)_2$ nanostructures in the degradation of Reactive Green 19A and textile effluent, phytotoxicity studies and their biogenic properties (antibacterial and anticancer), Journal of Environmental Management (2018), https://doi.org/10.1016/j.jenvman.2018.04.072